Nanoscale

Accepted Manuscript

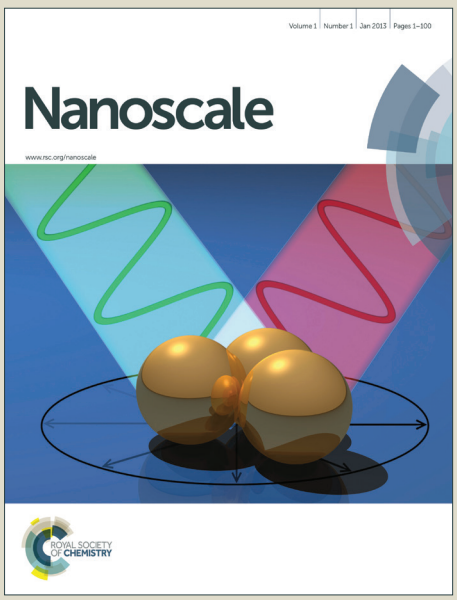

ROYAL SOCIETY OF CHEMISTRY

www.rsc.org/nanoscale

Cite this: DOI: 10.1039/c0xx00000x

www.rsc.org/xxxxxx

ARTICLE TYPE

Ultrasmall biomolecule-anchored hybrid $GdVO_4$ nanophosphors as a metabolizable multimodal bioimaging contrast agent

Kai Dong,[a,b] Enguo Ju,[a,b] Jianhua Liu,[c] Xueli Han,[c] Jinsong Ren*[a] and Xiaogang Qu*[a]

Received (in XXX, XXX) Xth XXXXXXXXX 20XX, Accepted Xth XXXXXXXXX 20XX

DOI: 10.1039/b000000x

Multimodal molecular imaging has recently attracted much attention on disease diagnostics due to taking advantage of individual imaging modalities. Herein, we demonstrated a new paradigm for multimodal bioimaging based on amino acids-anchored ultrasmall lanthanide-doped $GdVO_4$ nanoprobes. In merit of special metal-cation complexation and abundant functional groups, these amino acids-anchored nanoprobes would show high colloidal stability and excellent dispersibility. Additionally, due to typical paramagnetic behaviour, high X-ray mass absorption coefficient and strong fluorescence, these nanoprobes would provide a unique opportunity to develop multifunctional probes for MRI, CT and luminescence imaging. More importantly, the small size and biomolecule coatings endow the nanoprobes with the effective metabolism and high biocompatibility. With the superior stability, high biocompatibility, effective metabolism and excellent contrast performance, amino acids-capped $GdVO_4$:Eu^{3+} nanocastings were a promising candidate as multimodal contrast agents and would bring more opportunities for biological and medical applications with further modification.

1. Introduction

Along with the rapid development in nanotechnology and bioengineering, significant attention has been focused on developing disease diagnostic nanoprobes using modern imaging modalities, such as optical, ultrasound, magnetic resonance imaging (MRI), X-ray computed tomography (CT), positron emission tomography (PET), and photoacoustic tomography (PAT).[1-5] Among the various nanoparticulate contrast agents, the lanthanide-doped Gd^{3+}-containing nanoparticles have shown prominent potential in biomedical field.[6-11] Owing to the superior characteristics such as long luminescence lifetime, narrow emission band widths, high resistance to photobleaching, the lanthanide-doped Gd^{3+}-containing inorganic nanoparticles have become promising alternative to organic fluorophores and quantum dots for application in photoluminescent bioimaging.[12,13] Additionally, Gd^{3+} ions, with unpaired f electrons are paramagnetic and have been used as contrast agents for MR imaging.[14-17] Moreover, because of their relatively larger K-edge value and higher X-ray mass absorption coefficient, Gd^{3+}-doped nanocastings have been used as more excellent CT contrast agents than routinely used small iodinated molecules.[18-21] Given above, lanthanide-doped Gd^{3+}-containing nanoparticles would be applied as nanoprobes for multimodal imaging, combining CT, MRI and PL imaging, providing combined advantages of high temporospatial resolution and relatively high sensitivity. In particular, for application to in vivo bioimaging, there were some rigorous requirements for bioprobes, such as small size (<10 nm), metabolism and biocompatibility.[22-27] However, the formation of monodispersed sub-10 nm lanthanide-doped nanoparticles was generally based on high temperature thermal decomposition methods, which makes the hydrophobic ligands remain on the surface of nanoparticles. Therefore, for the biocompatible and practical utility, these as-prepared nanoagents always need to be functionalized with biocompatible molecules through complicated synthesis routes, time-consuming experiment techniques, and stringent synthetic conditions such as layer-by-layer method, post-modification of ion complex, as well as ligand exchange route.[28-32] Generally, several amphiphilic polymer materials have been chosen for surface coating and assemble with nanoparticles to form hydrophobic inner layer. In this way, the hydrophobic inner layer would restrict water exchange, reduce the r_1 relaxivity and weaken contrast effect.[33-35] Accordingly, fabrication of ultrasmall, metabolizable and biocompatible multimodal contrast agents via simple methods and achieving superior contrast effect are very challenging but highly desirable.

In recent years, as a new bottom-up solution chemistry method to design and manipulate desired structures, biomolecule-assisted synthetic routes have attracted much attention. Various biomolecules, such as DNA, proteins, peptides, and enzyme, have been exploited to become extremely favorable scaffolds for the fabrication of various nanoparticles, which have shown potential in catalysis, biosensing, clinical diagnosis and therapy, et al. [36-45] Taking advantage of biomolecular complexation, functional nanostructures can be prepared without additional complex modification. Additionally, biomolecule-assisted synthetic nanoparticles possess a large number of functional groups anchoring on their surface to enable solubility/dispersibility in various solvents. These functional groups can also allow flexible covalent chemistry for linkage with target molecules. More

significantly, biomolecule-capped nanoparticles have shown low toxicity and high biocompatibility for biomedical applications.

Herein, we demonstrated a new paradigm for multimodal bioimaging based on amino acids-anchored ultrasmall lanthanide-doped $GdVO_4$ nanoprobes. In merit of special metal-cation complexation and abundant functional groups, these amino acids-anchored nanoprobes would show high colloidal stability and excellent dispersibility in different media. Additionally, due to typical paramagnetic behavior, high X-ray mass absorption coefficient and strong fluorescence, these nanoprobes would provide a unique opportunity to develop multifunctional probes for MRI, CT and luminescence imaging. More importantly, the small size and biomolecule coatings would endow the nanoprobes with the effective metabolism and high biocompatibility, which is the emphasis on moving this contrast agent closer to the clinical setting.

2. Experimental section

2.1. Reagents and materials

All chemicals were of analytical grade and used directly without further purification. Gadolinium (III) nitrate hexahydrate ($Gd(NO_3)_3{\cdot}6H_2O$), europium(III) nitrate hexahydrate ($Eu(NO_3)_3{\cdot}6H_2O$), sodium orthovanadate (Na_3VO_4), aminoacetic acid (NH_2CH_2COOH) were purchased from Aladdin. Dehydrated ethanol was purchased from Beijing Chemicals (Beijing, China). Water throughout all experiments was obtained by using a Milli-Q water system.

2.2. Synthesis of amino acids-capped $GdVO_4$: Eu^{3+} nanocastings

$Gd(NO_3)_3{\cdot}6H_2O$ (0.2616 g), $Eu(NO_3)_3{\cdot}5H_2O$ (0.0136 g), and aminoacetic acid (0.16 g) were dissolved in 20 mL of distilled water. 20 mL of an aqueous Na_3VO_4 solution (0.1122 g) was added to the above aqueous solution under magnetic stirring for about 10 min at room temperature. The resulting reaction mixture (40 mL) was transferred to a Teflon-lined stainless steel autoclave and treated at desired temperature in the range of 180 ^oC for 20 h, and then cooled naturally to room temperature. The obtained product was centrifugated, washed several times by water and ethanol, and dried at 60 ^oC for 2 h.

2.3. Leaching study of Gd^{3+} ions from the nanoparticles

10 mL of $GdVO_4$: Eu^{3+} nanoparticles solution (1 mg/mL) was taken into a dialysis bag (50 kD cut-off) and dialyzed against physiological saline with 10% fetal bovine serum under stirring. Taking 0.5 mL of above physiological saline out one week later and inductively coupled plasma mass spectrometry (ICP-MS) was applied to determine the content of Gd^{3+} ions.

2.4. Cell cultures

A549 cells, HEK-293 cells and HeLa cells were supplied by ATCC (American Type Culture Collection). Cells were cultured in Dulbecco's modified Eagle's medium (DMEM) containing penicillin (100 U/mL), streptomycin (100 μg/mL), and 10% fetal bovine serum (FBS) in a humidified incubator at 37 ºC and 5% CO_2. Cells were harvested by the use of trypsin and were resuspended in fresh complete medium before plating.

2.5. In vitro cytotoxicity studies

MTT reduction assays were carried out to quantify the cytotoxicity of $GdVO_4$: Eu^{3+} nanocastings. In a typical procedure, cells (A549 and HEK-293 cell lines) were cultured in 96-well plates as a density of 5000 per well for 12 h to allow the cells to attach. Subsequently, serial dilutions of different nanoparticles formulations were added to the culture medium. At the end of the incubation time, the medium containing nanoparticles were removed, and cell samples were treated with MTT for another 4 h, which was followed by the addition of dimethyl sulfoxide (DMSO) to dissolve the formazan crystals. Bio-Rad model-680 microplate reader was applied to measure the absorbance at a wavelength of 570 nm (corrected for background absorbance at 630 nm). Six replicates were done for each treatment group and percent viability was normalized to cell viability in the absence of nanoparticles.

2.6. Cellular modality and observation

To observe morphological changes of cells, a typical experiment, A549 and HEK-293 cells with a density of 2×10^4 were placed in a 24-well plate for 4 h to allow the cells to attach. After the cells were washed twice by cool phosphate-buffered saline (PBS), nanoparticles (200 μg/mL) were added to the cell culture medium. After incubating for 48 h, the cells were washed again with PBS several times to remove the remaining nanoparticles, and then observed under an Olympus BX-51 optical system microscopy upon white light. Pictures were then taken with an Olympus digital camera.

2.7. In vitro hemolysis assay

The hemolysis assay experiments were carried out as an important factor to evaluate the in vitro biocompatibility. Human blood samples stabilized by EDTA were obtained from the local hospital. Firstly, 1 mL of blood sample was added to 2 mL of PBS, and then red blood cells (RBCs) were isolated from serum by centrifugation at 8,000 rpm for 10 min. After being washed five times with 5 mL of PBS solution, the purified blood was diluted to 1/10 of its volume with PBS solution. 0.2 mL of diluted RBC suspension was then mixed with (a) 0.8 mL of PBS as a negative control, (b) 0.8 mL of D. I. water as a positive control, and (c) 0.8 mL of $GdVO_4$: Eu^{3+} nanoparticle suspensions at concentrations ranging from 0 to 200 μg mL^{-1}. Then all the mixtures were vortexed and kept at room temperature for 3 h. Finally, the mixtures were centrifuged at 8,000 rpm for 5 min, the absorbance of supernatants at 541 nm was determined by a JASCO V-550 UV-vis spectroscopy. The percent hemolysis of RBCs was calculated as following: percent hemolysis = [(sample absorbance – negative control absorbance) / (positive control absorbance – negative control absorbance)] × 100.

2.8. In vitro phosphorescence imaging

HeLa cells were incubated with $GdVO_4$: Eu^{3+} nanoparticles (100 μg/mL) for 4 h, and were washed with phosphate buffer saline (PBS) three times and being resupplied with fresh DMEM. Phosphorescence images were collected. The cell samples were then examined by an Olympus BX-51 optical system microscopy. Pictures were taken with an Olympus digital camera.

2.9. Animal administration

Wistar rats and Kunming mice were purchased from Medical Experimental Animal Center of Jilin University (Changchun, China). All animal procedures were in accord with the guidelines of the Institutional Animal Care and Use Committee.

2.10. In vitro and in vivo CT imaging

For in vitro CT imaging, $GdVO_4$: Eu^{3+} nanoparticles and Iobitridol were dispersed in PBS buffer solution at concentrations ranging from 0 to 100 mM. For in vivo CT imaging, the rat was first anesthetized by intraperitoneal injection of chloral hydrate solution (10 wt%), and then 1 mL of $GdVO_4$: Eu^{3+} nanoparticles solution (25 mM) were injected intravenously into rat, respectively. The rat was imaged repeatedly up to 60 min. CT images were collected using a JL U.A NO.2 HOSP Philips iCT 256 slice scanner, imaging parameters were as follows: thickness, 0.9 mm; pitch, 0.99; 120 KVp, 300 mA; field of view, 350 mm; gantry rotation time, 0.5 s; table speed, 158.9 mm/s.

2.11. In vitro and in vivo MR imaging

For in vitro T_1-weighted MR imaging, dilutions of $GdVO_4$: Eu^{3+} nanoparticles in PBS buffer solution containing 1% agarose with expected different concentrations as contrast agent were placed in a series of Eppendorf tubes for T_1-weighted MR imaging. After careful preparation, the Eppendorf tubes were then scanned in a 1.5 T Magnetom Espree MIR system (Siemens). For in vivo MRI, the rat was first anesthetized by intraperitoneal injection of chloral hydrate solution (10 wt%), and then 1 mL of $GdVO_4$: Eu^{3+} nanoparticles dispersion in PBS buffer solution with 10 mM of Gd was administrated intravenously into a rat. The T_1-weighted images were acquired using a 1.5 T human clinical scanner.

2.12. Biodistribution assays

To study the tissue distribution for $GdVO_4$: Eu^{3+} nanoparticles, the organs (heart, liver, spleen, lung, and kidneys) were surgically removed at various times (post-2 h, 24 h, 7 days, 30 days) after delivery the nanorods by injection through the tail vein. The Gd ions were quantified through ICP-MS method. The organs were surgically removed from the animal and placed into a centrifuge tube containing 4 mL of aqua regia, and then incubated for 2 h under heat treatment (80 ºC) for dissolution of the tissues. The obtained liquid was subjected to ICP-MS analysis.

2.13. Hematology studies

$GdVO_4$: Eu^{3+} nanoparticles (5 mg/kg) was injected via the tail vein into five healthy Kunming mice in each group, other five mice were used as the untreated controls. 30 days after injection, mice in each group were respectively sacrificed to collect blood (0.8 mL) for serum biochemistry assay and complete blood panel test.

2.14. Histologic analysis

For histologic studies, mice were sacrificed for 30 days after administration. The tissues (heart, spleen, liver, lung, and kidney) were collected from above two groups (control and test groups). The ex vivo organics were immersed in a buffered solution of 4% paraformaldehyde for 2-3 days, dehydrated and treated for inclusion in paraffin. The specimen was sectioned serially at 4 mm thickness and stained with hematoxylin and eosin (H&E). The histological sections were observed under an optical microscope.

2.15. Statistical analysis

All data were expressed in this article as mean result ± standard deviation (SD). All figures shown in this article were obtained from three independent experiments with similar results. The statistical analysis was performed by using Origin 8.0 software.

2.16. Characterization

Transmission electron microscope (TEM) measurements were carried out on a JEOL JEM-2010EX transmission electron microscope with a tungsten filament at an accelerating voltage of 200 kV. Energy-dispersive X-ray spectrometer (EDS) was employed for approximate elemental analyses. The samples were prepared by placing a drop of prepared solution on the surface of a copper grid and dried at room temperature. The crystalline structures of the as-prepared samples were evaluated by X-ray diffraction (XRD) analysis on a Rigaku-Dmax 2500 diffractometer by using $Cu_{K\alpha}$ radiation (λ = 0.15405 nm). The operation voltage and current were kept at 40 kV and 40 mA. The surface composition of the samples and binding energy were determined by X-ray photoelectron spectroscopy (XPS, Perkin Elmer PHI 5600). FT-IR analyses were carried out on a Bruker Vertex 70 FT-IR Spectrometer

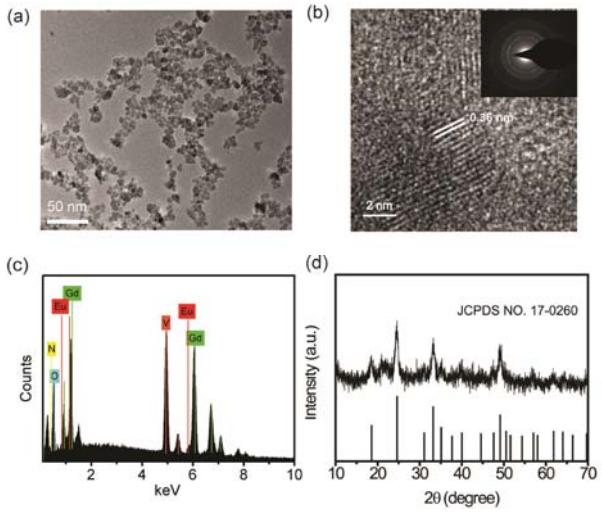

Fig. 1 (a) TEM image of amino acids-capped $GdVO_4$:Eu^{3+} nanoparticles. (b) High-resolution TEM of the as-prepared nanoparticles. Inset of (b): SAED of the products. (c) EDS spectrum and (d) wide-angle XRD pattern of as-prepared nanoparticles.

3. Results and discussion

In attempting to obtain multimodal imaging nanoprobes, aminoacetic acid was used as template to assist one-step hydrothermal synthesis of $GdVO_4$:Eu^{3+} nanocastings. The morphology of as-prepared amino acids-anchored $GdVO_4$:Eu^{3+} nanoparticles were observed by TEM. As shown in Fig. 1a, monodisperse and uniform sphere-like nanoparticles have been successfully constructed and the average diameter was approximately 6 nm (Fig. S1a). The hydrodynamic diameter of $GdVO_4$:Eu^{3+} nanoparticle was also measured by dynamic light

scattering (DLS) (Fig. S1b). The diameters of as-prepared amino acids-anchored $GdVO_4:Eu^{3+}$ based on DLS became larger than the size observed from TEM images due to the swell in aqueous solution. High-resolution TEM images suggested that the nanoparticle was a single crystal with an interplanar spacing of 0.30 nm, which corresponds to the separation between the (200) lattice planes of tetragonal $GdVO_4$ (Fig. 1b). The elemental dispersive spectrum (EDS) evidenced the existence of all expected elements (Gd, Eu, V, O and N) in the as-prepared nanoparticles (Fig. 1c). All of the diffraction peaks' positions and intensities for the as-prepared nanoparticles in the X-ray diffraction (XRD) pattern (Fig. 1d) were in good agreement with the reference data (JCPDs: 17-0260). In addition, carboxylic groups were observed from the Fourier transform infrared (FTIR) spectrum, which demonstrated that amino acids were anchored on the surface of the nanoparticles (Fig. S2). The amount of amino acids on the nanoparticles, as evaluated by TGA analysis, was approximately 6.20% (Fig. S3). Due to the present of hydrophilic ligands on their surface, the well-designed products were stable and dispersible in various solutions including PBS, FBS, and DMEM, which was important for further biomedical application (Fig. S4).

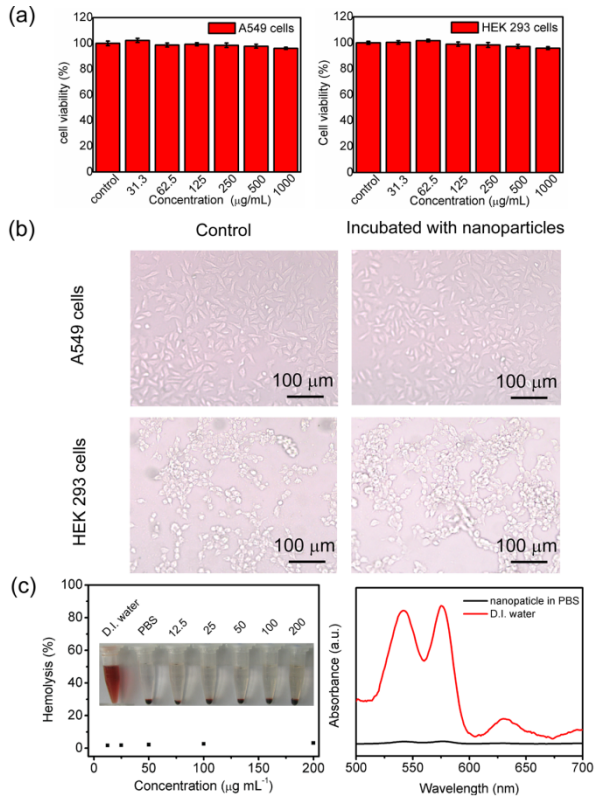

Fig. 2 (a) Cell viability of A549 cells and HEK 293 after incubation with increased concentration of $GdVO_4:Eu^{3+}$ nanoparticles for 24 h. (b) Microscope images of the A549 cells and HEK 293 incubated without and with $GdVO_4:Eu^{3+}$ nanoparticles for 24 h. (c) Concentration-dependent hemolysis of $GdVO_4:Eu^{3+}$ nanoparticles and UV-vis absorption spectra to detect the presence of hemoglobin in the supernatant of nanoparticles. Inset: photographic images for direct observation of hemolysis.

To evaluate the potential application of amino acids-capped $GdVO_4:Eu^{3+}$ nanoparticles as multimodal bioimaging probes, the toxicity of nanomaterials were firstly investigated. Leaching of free Gd ions from materials could cause high toxicity towards natural organs and tissue, such as nephrogenic systemic fibrosis (NSF), thereby long-term dialysis experiments against solution were initially studied.[46,47] The result revealed that no significant leakage of Gd^{3+} was measured through inductively coupled plasma mass spectrometry (ICP-MS) even after a week, which was benefit from the functional groups (amines and carbonyls) interacted with the metal ions.

Having established the excellent dispersibility and stability of the amino acids-anchored $GdVO_4:Eu^{3+}$ nanocastings in solution, we next performed methyl thiazolyl tetrazolium (MTT) assay to evaluate their cytotoxicity with A549 cells and HEK 293 cells, which determined their feasibility for potential bioimaging applications. After incubation with increasing amounts of $GdVO_4:Eu^{3+}$ nanoparticles for 24 h, neither the cell viability nor proliferation in A549 cells and HEK 293 cells were hindered. Even at a relatively high dose of nanoparticles (1000 μg/mL), the cell viability still remained above 90% (Fig. 2a). Morphological changes in living cells affected by $GdVO_4:Eu^{3+}$ were also investigated using microscope (Fig. 2b). Microscope images illustrated no obvious difference in the cell morphology between treated and control groups. In vitro hemolytic assay was usually applied to investigate the interaction between nanomaterials and blood components. As shown in Fig. 2c, nearly no signal around 541 nm was detected upon the maximal experimental concentration (200 μg/mL), indicating the extremely low hemolysis of amino acids-capped $GdVO_4:Eu^{3+}$ nanocastings. On the basis of these results, it could be inferred that amino acids-capped $GdVO_4:Eu^{3+}$ nanocastings was biocompatible and nearly nontoxic to live cells, which implied that they could serve as a secure contrast agent for bioimaging.

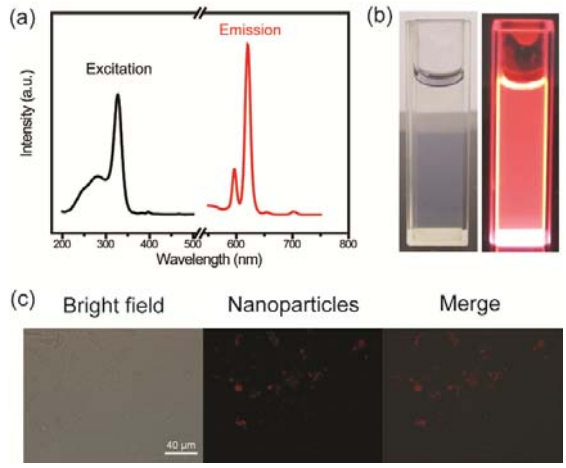

Fig. 3 (a) Phosphorescence spectrum of $GdVO_4:Eu^{3+}$ nanoparticles. (b) The photographs of $GdVO_4:Eu^{3+}$ nanoparticles under daylight and UV light. (c) Microscopic images of HeLa cell incubated with $GdVO_4:Eu^{3+}$ nanoparticles.

Compared with organic luminophores, phosphorescent lanthanide-doped complexes as probes have attracted increasing interest due to their advantageous photophysical properties, such as large Stoke's shifts for easy separation of excitation and emission, high photostability, and long emission-lifetimes.[48]

Hence, phosphorescent probes based on lanthanide-doped nanocomplexes are very promising for applications in sensing and bioimaging. Excitation and emission spectra of amino acids-capped $GdVO_4:Eu^{3+}$ nanoparticles showed in Fig. 3a. The nanoprobes exhibited absorption at 330 nm, and emitted intense red phosphorescence at 620 nm in aqueous solutions. As can be seen in Fig. 3b, the colloidal solutions of the nanoparticles showed bright red luminescence when excited with a UV lamp. Additionally, the phosphorescence decay of the emission that the dominant lifetime of the nanopartilces was 0.90 ms (Fig. S5), which was considerably long compared with those of available organic luminophores. With intense red phosphorescence and long life time, the ability of amino acids-capped $GdVO_4:Eu^{3+}$ nanoparticles serving as bioprobes for cellular imaging was investigated. As shown in Fig. 3c, after HeLa cells were incubated with $GdVO_4:Eu^{3+}$ nanoparticles (100 μg/mL) for 2 h at 37 °C, bright phosphorescence signals (red color) inside cells were observed. This result demonstrated that amino acids-capped $GdVO_4:Eu^{3+}$ nanoparticles can be used as a novel phosphorescent probe for the cellular imaging.

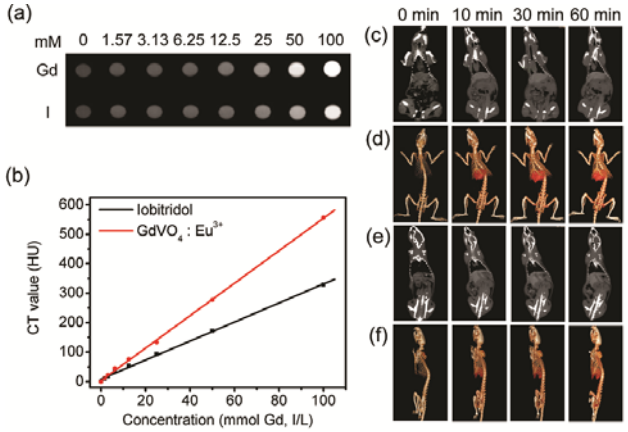

Fig. 4 (a) In vitro CT images of $GdVO_4:Eu^{3+}$ nanoparticles and iobitridol with different concentrations. (b) CT values (HU) of $GdVO_4:Eu^{3+}$ nanoparticles and iobitridol as a function of the agent concentrations at 120 KVp. (c-e) In vivo CT coronal view images of a rat after intravenous injection of 1 mL 25 mM $GdVO_4:Eu^{3+}$ nanoparticles solution at timed intervals. (c) Heart and liver. (e) Spleen and kidney. (d, f) The corresponding 3D renderings of in vivo CT images.

Owing to high X-ray mass attenuation coefficient (3.11 $cm^2\ g^{-1}$ at 100 keV) and large K-edge energy (50.2 keV), Gd-based nanostructures hold great promise as CT contrast agents. To investigate the in vitro CT contrast efficacy, we compared the X-ray absorption of amino acids-capped $GdVO_4:Eu^{3+}$ nanoparticles to that of Iobitridol, a routinely used clinical CT contract agent (Fig. 4a). The Hounsfield units (HU) values varied linearly as a function of the each agent concentration (Fig. 4b). Notably, at equivalent concentrations, the measured HU value of amino acids-capped $GdVO_4:Eu^{3+}$ nanoparticles was significantly enhanced compared to Iobitridol due to the fact that the attenuation coefficient of Gd was larger than that of I (1.94 $cm^2\ g^{-1}$ at 100 keV). Moreover, lanthanides usually gave high HU value at clinical voltage because of both their high atomic number and suitable K-edge locating within the higher energy region of clinical X-ray spectrum. Therefore, our well-prepared nanoparticles showed greatly superior to previous reported Au-, Ta-, and W-based nanoparticulate contrast agents.[41, 49-51]

Encouraged by their high CT contrast performance of in vitro experiment, we further evaluated the feasibility of as-prepared nanoparticles as a CT contrast agent in vivo. We tested the whole-body CT imaging by intravenous injection of nanoparticles and discussed the biodistribution of contrast agents tracked by X-ray CT technique at timed intervals. As shown in Fig. 4c and 4d, we could observe clear contrast enhancement in liver at an early time (10 min) and a gradual accumulation in the liver as time progressed. Remarkably, even after 1 h, the HU value of the liver was still higher than other surrounding tissues. This feature of the long-lasting liver contrast enhancement was mainly ascribed to the fact that more nanoparticles could be accumulated by macrophages and hepatocytes. These results indicated that our imaging nanoprobe was beneficial in potential clinical applications because of its highly stability and excellent contrast performance.

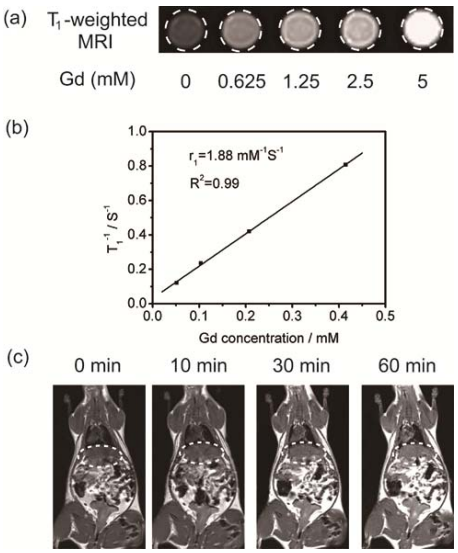

Fig. 5 (a) In vitro T1-weighted MRI image of $GdVO_4:Eu^{3+}$ nanoparticles with different concentrations. (b) Plot of $1/T_1$ versus Gd concentration. The slope indicates the specific relaxivity (r_1). (c) In vivo coronal view MRI images of a rat after intravenous injection of $GdVO_4:Eu^{3+}$ nanoparticles solution at different time intervals.

Simultaneously, because the Gd in $GdVO_4:Eu^{3+}$ nanoparticles can accelerate longitudinal (T_1) relaxation of water protons, the nanoprobes were expected to act as a T_1-weighted MRI contrast agent. To verify the MRI effectiveness of nanoprobes, an in vitro T_1-weighted MR imaging was conducted on a 1.5 T Siemens Magnetom Trio system. As illustrated in Fig. 5a, a positive enhancement for MR signal was observed for all the tubes comparing to water. Moreover, with the increase of $GdVO_4:Eu^{3+}$ nanoparticles concentration, T_1-weighted MR imaging intensity substantially brightened, demonstrating it could serve as an efficient T_1-weighted MR contrast agent. The specific relaxivity values (r_1) calculated from the slope of the concentration-dependent relaxation rate was 1.88 $mmol^{-1}s^{-1}$, which was comparable to the values of previous Gd-based T_1 contrast agents (Fig. 5b).[52-55]

Additionally, the application of MR imaging in vivo for small animals was also demonstrated by the rat after intravenous injection with 1 mL 10 mM $GdVO_4:Eu^{3+}$ nanoparticles. The pre-contrast and post-contrast T_1-weighted MR imaging were recorded at the beginning, and after 10 min, 30 min, and 60 min following injection with nanoparticles. It was worth noting that the nanoprobes could induce an efficient positive-contrast enhancement in liver along with the passing of time (Fig. 5c), which was consistent with our CT imaging results. These results suggested that the as-prepared nanoprobes could be desirable contrast agents for MR imaging.

With the excellent multifunctional imaging performance of amino acids-capped $GdVO_4:Eu^{3+}$ nanoparticles, detailed toxicity in vivo must be well investigated before they are translated into the clinic. [55-59] As shown in Fig. 6a, nearly no $GdVO_4:Eu^{3+}$ nanoparticles retained in the mice body at one month after administration of a single dose, indicating the effective time-dependent metabolism process. In order to know the pathway of the $GdVO_4:Eu^{3+}$ nanoparticles clearance from the mice body, the accurate biodistribution of the contrast agent in the main organs (heart, liver, spleen, lung, kidneys, and intestine) was measured as a function of time and detected through ICP-MS analysis. As shown in Fig. 6b, markedly decreasing signals of Gd^{3+} contents in all organs were observed due to the stepwise clearance of nanoparticles from mice body. Furthermore, Gd content measurements in mice excretions (feces and urine) after intravenous injection showed that the contrast agent was possibly through both renal and fecal excretions and could be easily excreted via metabolism (Fig. S6).

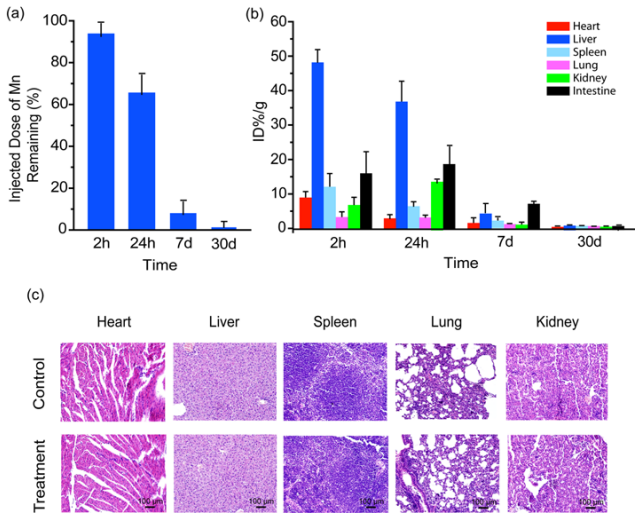

Fig. 6 (a) Whole body clearance of $GdVO_4:Eu^{3+}$ nanoparticles in mice at different timed intervals. (b) Time-dependent biodistribution of $GdVO_4:Eu^{3+}$ nanoparticles in mice. (c) Histological changes of the mice 30 days after a single-dose intravenous injection of $GdVO_4:Eu^{3+}$ nanoparticles. These organs are stained with H&E and observed under a light microscope. Error bars were based on standard deviation of 5 mice per group.

To further determine whether $GdVO_4:Eu^{3+}$ nanoparticles caused any adverse effects or disease during its retention in the mice bodies, we next investigated the long-term toxicity through body weight measurement, histological assessment and hematology analysis. The fluctuation in body weight is a useful indicator for studying the toxicity effects. As shown in Fig. S7, body weight of the test group increased slightly in a pattern similar to that of the control group. Straightforward behavior observation over 30 days also indicated that there were no obvious signals of toxicity. Additionally, histological assessment was performed on the tissues obtained from the susceptible organs (heart, liver, spleen, lung, and kidney) to assess signs of potential toxicity. As shown in Fig. 6c, no tissue damage or any other harmful effect associated with the administration of the contrast agents was observed compared with those of the control group after the hematoxylin and eosin (H&E) stain. Otherwise, the structures of organs from the exposed mice were as normal as those of control group (Fig. S8). For hematology analysis and blood biochemical assay, there was nearly no difference between these two groups one month after intravenous injection (Table S1). Based on above results, it indicated that amino acids-assisted $GdVO_4:Eu^{3+}$ nanoparticles showed promise as a multimodal contrast agent for applications in biological medicine because of their eminent safety.

4. Conclusions

In summary, ultrasmall $GdVO_4:Eu^{3+}$ nanoprobes were successfully synthesized by amino acids-assisted approach and used as a new platform for MRI/CT/phosphorescence multimodal imaging. Amino acids endowed nanoparticles with high colloidal stability and excellent dispersibility. Additionally, toxicity studies results revealed the excellent biocompatibility of $GdVO_4:Eu^{3+}$ nanoparticles, indicating the feasibilities for bioimaging. The property of phosphorescence, which possessed the strong red light emission, enhanced the high signal-to-noise ratio of cellular imaging. Moreover, Gd in amino acids-capped $GdVO_4:Eu^{3+}$ nanoparticles endowed the nanoprobes with high longitudinal relaxivity and the nanoparticles were suitable for T_1-weighted MR imaging. Notably, by virtue of a high X-ray absorption coefficient and a high content of gadolinium, the well-prepared nanoprobes provided a higher contrast efficacy than routine iodine-based agents in clinic. More importantly, the study of pharmacokinetics, biodistribution, and in vivo toxicology demonstrated the nanoprobes possessed effective metabolism and high biocompatibility. With the superior stability, high biocompatibility, effective metabolism and excellent contrast performance, amino acids-capped $GdVO_4:Eu^{3+}$ nanocastings were a promising candidate as in vivo multimodal contrast agents and would bring more opportunities for biological and medical applications with further modification.

Acknowledgements

Financial support was provided by the National Basic Research Program of China (Grant 2012CB720602, 2011CB936004) and the National Natural Science Foundation of China (Grants 91213302, 21210002).

Notes and references

[a] *State Key Laboratory of Rare Earth Resource Utilization and Laboratory of Chemical Biology, Changchun Institute of Applied*

Chemistry, Changchun, Jilin 130022 (China). E-mail: jren@ciac.ac.cn; xqu@ciac.ac.cn
[b] *University of the Chinese Academy of Sciences, Beijing 100039 (China).*
[c] *Department of Radiology, the Second Hospital of Jilin University, Changchun, Jilin 130022 (China).*
† Electronic Supplementary Information (ESI) available. See DOI: 10.1039/b000000x/

1. J. Kim, Y. Piao and T. Hyeon, Chem. Soc. Rev., 2009, 38, 372-390.
2. A. Y. Louie, *Chem. Rev.*, 2010, **110**, 3146-3195.
3. J. Zhou, Z. Liu and F. Y. Li, *Chem. Soc. Rev.*, 2012, **41**, 1323-1349.
4. J. Xie, G. Liu, H. S. Eden, H. Ai and X. Y. Chen, *Acc. Chem. Res.*, 2011, **44**, 883-892.
5. Y. S. Liu, D. T. Tu, H. M. Zhu and X. Y. Chen, *Chem. Soc. Rev.*, 2013, **42**, 6924-6958.
6. A. Xia, M. Chen, Y. Gao, D. M. Wu, W. Feng and F. Y. Li, *Biomaterials*, 2012, **33**, 5394-5405.
7. Z. Liu, F. Pu, S. Huang, Q. H. Yuan, J. S. Ren and X. G. Qu, *Biomaterials*, 2013, **34**, 1712-1721.
8. J. Zhou, Z. G. Lu, G. G. Shan, S. H. Wang and Y. Liao, *Biomaterials*, 2014, **35**, 368-377.
9. Z. Liu, X. Liu, Q. H. Yuan, K. Dong, L. Y. Jiang, Z. Q. Li, J. S. Ren and X. G. Qu, *J. Mater. Chem.*, 2012, **22**, 14982-14990.
10. L. Cheng, K. Yang, Y. G. Li, X. Zeng, M. W. Shao, S. T. Lee and Z. Liu, *Biomaterials*, 2012, **33**, 2215-2222.
11. H. Y. Xing, W. B. Bu, S. J. Zhang, X. P. Zheng, M. Li, F. Chen, Q. J. He, L. P. Zhou, W. J. Peng, Y. Q. Hua and J. L. Shi, *Biomaterials*, 2012, **33**, 1079-1089.
12. F. Wang, R. R. Deng, J. Wang, Q. X. Wang, Y. Han, H. M. Zhu, X. Y. Chen and X. G. Liu, *Nat. Mater.*, 2011, **10**, 968-973.
13. A. Kar and A. Patra, *Nanoscale*, 2012, **4**, 3608-3619.
14. H. B. Na, I. C. Song and T. Hyeon, *Adv. Mater.*, 2009, **21**, 2133-2148.
15. T. Courant, V. G. Roullin, C. Cadiou, M. Callewaert, M. C. Andry, C. Portefaix, C. Hoeffel, M. C. de Goltstein, M. Port, S. Laurent, L. Vander Elst, R. Muller, M. Molinari and F. Chuburu, *Angew. Chem. Int. Ed.*, 2012, **51**, 9119-9122.
16. C. C. Huang, C. H. Su, W. M. Li, T. Y. Liu, J. H. Chen and C. S. Yeh, *Adv. Funct. Mater.*, 2009, **19**, 249-258.
17. J. L. Bridot, A. C. Faure, S. Laurent, C. Riviere, C. Billotey, B. Hiba, M. Janier, V. Josserand, J. L. Coll, L. Vander Elst, R. Muller, S. Roux, P. Perriat and O. Tillement, *J. Am. Chem. Soc.*, 2007, **129**, 5076-5084.
18. A. Jakhmola, N. Anton and T. F. Vandamme, *Adv. Healthc. Mater.*, 2012, **1**, 413-431.
19. N. Lee, S. H. Choi and T. Hyeon, *Adv. Mater.*, 2013, **25**, 2641-2660.
20. S. B. Yu and A. D. Watson, *Chem. Rev.*, 1999, **99**, 2353-2377.
21. S. J. Zeng, M. K. Tsang, C. F. Chan, K. L. Wong and J. H. Hao, *Biomaterials*, 2012, **33**, 9232-9238.
22. Q. Liu, Y. Sun, T. S. Yang, W. Feng, C. G. Li and F. Y. Li, *J. Am. Chem. Soc.*, 2011, **133**, 17122-17125.
23. Q. Ju, D. T. Tu, Y. S. Liu, R. F. Li, H. M. Zhu, J. C. Chen, Z. Chen, M. D. Huang and X. Y. Chen, *J. Am. Chem. Soc.*, 2012, **134**, 1323-1330.
24. Y. S. Liu, S. Y. Zhou, D. T. Tu, Z. Chen, M. D. Huang, H. M. Zhu, E. Ma and X. Y. Chen, *J. Am. Chem. Soc.*, 2012, **134**, 15083-15090.
25. J. Y. Park, M. J. Baek, E. S. Choi, S. Woo, J. H. Kim, T. J. Kim, J. C. Jung, K. S. Chae, Y. Chang and G. H. Lee, *Acs Nano*, 2009, **3**, 3663-3669.
26. Q. W. Tian, J. Q. Hu, Y. H. Zhu, R. J. Zou, Z. G. Chen, S. P. Yang, R. W. Li, Q. Q. Su, Y. Han and X. G. Liu, *J. Am. Chem. Soc.*, 2013, **135**, 8571-8577.
27. J. B. Liu, M. X. Yu, C. Zhou, S. Y. Yang, X. H. Ning and J. Zheng, *J. Am. Chem. Soc.*, 2013, **135**, 4978-4981.
28. H. Schafer, P. Ptacek, O. Zerzouf and M. Haase, *Adv. Funct. Mater.*, 2008, **18**, 2913-2918.
29. L. L. Li, R. B. Zhang, L. L. Yin, K. Z. Zheng, W. P. Qin, P. R. Selvin and Y. Lu, *Angew. Chem. Int. Ed.*, 2012, **51**, 6121-6125.
30. Y. M. Yang, Q. Shao, R. R. Deng, C. Wang, X. Teng, K. Cheng, Z. Cheng, L. Huang, Z. Liu, X. G. Liu and B. G. Xing, *Angew. Chem. Int. Ed.*, 2012, **51**, 3125-3129.
31. G. Tian, Z. J. Gu, L. J. Zhou, W. Y. Yin, X. X. Liu, L. Yan, S. Jin, W. L. Ren, G. M. Xing, S. J. Li and Y. L. Zhao, *Adv. Mater.*, 2012, **24**, 1226-1231.
32. N. Bogdan, F. Vetrone, G. A. Ozin and J. A. Capobianco, *Nano Lett.*, 2011, **11**, 835-840.
33. R. J. Xing, F. Zhang, J. Xie, M. Aronova, G. F. Zhang, N. Guo, X. L. Huang, X. L. Sun, G. Liu, L. H. Bryant, A. Bhirde, A. Liang, Y. L. Hou, R. D. Leapman, S. H. Sun and X. Y. Chen, *Nanoscale*, 2011, **3**, 4943-4945.
34. J. Huang, J. Xie, K. Chen, L. H. Bu, S. Lee, Z. Cheng, X. G. Li and X. Y. Chen, *Chem. Commun.*, 2010, **46**, 6684-6686.
35. B. Y. W. Hsu, M. Wang, Y. Zhang, V. Vijayaragavan, S. Y. Wong, A. Y. C. Chang, K. K. Bhakoo, X. Li and J. Wang, *Nanoscale*, 2014, **6**, 293-299.
36. J. Sharma, R. Chhabra, A. Cheng, J. Brownell, Y. Liu and H. Yan, *Science*, 2009, **323**, 112-116.
37. N. Ma, E. H. Sargent and S. O. Kelley, *Nat. Nanotechnol.*, 2009, **4**, 121-125.
38. L. Zhou, Z. H. Li, E. G. Ju, Z. Liu, J. S. Ren and X. G. Qu, *Small*, 2013, **9**, 4262-4268.
39. T. D. Nguyen, D. Mrabet, T. T. D. Vu, C. T. Dinh and T. O. Do, *Crystengcomm*, 2011, **13**, 1450-1460.
40. S. J. Ding, Y. M. Wang, Z. L. Hong, X. J. Lu, D. Y. Wan and F. Q. Huang, *Chem-Eur J.*, 2011, **17**, 11535-11541.
41. K. Dong, Z. Liu, J. H. Liu, S. Huang, Z. H. Li, Q. H. Yuan, J. S. Ren and X. G. Qu, *Nanoscale*, 2014, **6**, 2211-2217.
42. L. Zhou, Z. H. Li, Z. Liu, M. L. Yin, J. S. Ren and X. G. Qu, *Nanoscale*, 2014, **6**, 1445-1452.
43. C. L. Liu, H. T. Wu, Y. H. Hsiao, C. W. Lai, C. W. Shih, Y. K. Peng, K. C. Tang, H. W. Chang, Y. C. Chien, J. K. Hsiao, J. T. Cheng and P. T. Chou, *Angew. Chem. Int. Ed.*, 2011, **50**, 7056-7060.
44. Y. Tao, Z. H. Li, E. G. Ju, J. S. Ren and X. G. Qu, *Chem. Commun.*, 2013, **49**, 6918-6920.
45. M. Colombo, S. Mazzucchelli, V. Collico, S. Avvakumova, L. Pandolfi, F. Corsi, F. Porta and D. Prosperi, *Angew. Chem. Int. Ed.*, 2012, **51**, 9272-9275.
46. J. G. Penfield and R. F. Reilly, *Nat. Clin. Pract. Nephr.*, 2007, **3**, 654-668.
47. C. Canavese, M. C. Mereu, S. Aime, E. Lazzarich, R. Fenoglio, M. Quaglia and P. Stratta, *J. Nephrol.*, 2008, **21**, 324-336.
48. F. Wang and X. G. Liu, *Acc. Chem. Res.*, 2014, **47**, 1378-1385.
49. H. Wang, L. F. Zheng, C. Peng, R. Guo, M. W. Shen, X. Y. Shi and G. X. Zhang, *Biomaterials*, 2011, **32**, 2979-2988.
50. M. H. Oh, N. Lee, H. Kim, S. P. Park, Y. Piao, J. Lee, S. W. Jun, W. K. Moon, S. H. Choi and T. Hyeon, *J. Am. Chem. Soc.*, 2011, **133**, 5508-5515.
51. L. Cheng, J. J. Liu, X. Gu, H. Gong, X. Z. Shi, T. Liu, C. Wang, X. Y. Wang, G. Liu, H. Y. Xing, W. B. Bu, B. Q. Sun and Z. Liu, *Adv. Mater.*, 2014, **26**, 1886-1893.
52. Y. L. Liu, K. L. Ai, J. H. Liu, Q. H. Yuan, Y. Y. He and L. H. Lu, *Angew. Chem. Int. Ed.*, 2012, **51**, 1437-1442.
53. R. Kumar, M. Nyk, T. Y. Ohulchanskyy, C. A. Flask and P. N. Prasad, *Adv. Funct. Mater.*, 2009, **19**, 853-859.
54. J. Zhou, M. X. Yu, Y. Sun, X. Z. Zhang, X. J. Zhu, Z. H. Wu, D. M. Wu and F. Y. Li, *Biomaterials*, 2011, **32**, 1148-1156.
55. L. Q. Xiong, T. S. Yang, Y. Yang, C. J. Xu and F. Y. Li, *Biomaterials*, 2010, **31**, 7078-7085.
56. Z. Liu, C. Davis, W. B. Cai, L. He, X. Y. Chen and H. J. Dai, *P. Natl. Acad. Sci. USA*, 2008, **105**, 1410-1415.
57. Z. Liu, S. M. Tabakman, Z. Chen and H. J. Dai, *Nat. Protoc.*, 2009, **4**, 1372-1382.
58. B. Wang, X. He, Z. Y. Zhang, Y. L. Zhao and W. Y. Feng, *Acc. Chem. Res.*, 2013, **46**, 761-769.
59. L. Cheng, K. Yang, M. W. Shao, X. H. Lu and Z. Liu, *Nanomedicine-Uk*, 2011, **6**, 1327-1340.